Volume 9, Issue 4, 2019, 4164 - 4167 ISSN 2069-5837

Biointerface Research in Applied Chemistry

www.BiointerfaceResearch.com

https://doi.org/10.33263/BRIAC94.164167

Original Research Article Open Access Journal

Received: 04.07.2019 / Revised: 04.08.2019 / Accepted: 09.08.2019 / Published on-line: 15.08.2019

Superparamagnetic and photocatalytic activity of $CoCe_{0.02}Dy_{0.02}Fe_{1.96}O_4$ nanoparticles synthesized by citrate-gel autocombustion technique

Mohd Hashim[1], Kadiyala Chandra Babu Naidu[2], G. Helen Ruth Joice[3], J. Laxman Naik[4], Dachepalli Ravinder[5,*]

[1]Department of Applied Physics, Aligarh Muslim University, Aligarh 202002, India
[2]Department of Physics, GITAM Deemed to be University, Bangalore-562163, Karnataka, India
[3]Thiru Kollanjiappar Arts College, Vriddhachalam-606001, Cuddalore Dist, Tamilnadu, India
[4]Department of Physics, University College of Science, Saifabad, Hyderabad- 500004, Osmania University, Telangana, India
[5]Department of Physics Osmania University, Hyderabad, 500007, Telangana, India

*corresponding author e-mail address:***ravindergupta28@rediffmail.com**

ABSTRACT

Mitigating organic pollutants by employing semiconducting materials is considered to be green and sustainable route to tackle the environmental problems. Herein, citrate-gel autocombustion method was adopted to synthesize Ce and Dy doped $CoFe_2O_4$ and characterized by various analytical techniques. The efficacy of prepared $CoCe_xDy_xFe_{2-2x}O_4$ (x=0-0.04) samples were tested for degradation of Methylene blue **(**MB) under visible light irradiation. The photocatalytic efficiency of $CoCe_{0.02}Dy_{0.02}Fe_{1.96}O_4$ for degradation of MB was found to be larger than pure $CoFe_2O_4$, Degussa P25 and other modified $CoFe_2O_4$. The enhanced photocatalytic activity was attributed to improved charge separation and visible light utilization by Ce and Dy into $CoFe_2O_4$ system. The super-spin glass behaviour of $CoCe_xDy_xFe_{2-2x}O_4$ confirmed from flat nature of magnetization of FC curve below T_B.

Keywords: *Nanoparticle; Magnetic; Photocatalysis; Rare Earth.*

1. INTRODUCTION

Methylene blue is one of the most representative organic dyes and it has been widely used in colorant industries. The direct discharge of such effluent in water body causes water pollution and poses a pervasive threat to aquatic system [1]. Semiconductor based technology which utilizes solar energy for the mineralization of textile pollutants has been considered as a green and viable strategy [2]. Many visible light sensitive photocatalysts such as $BiVO_4$, Bi_2O_3 Bi_2WO_6, WO_3 and Fe_3O_4 have been employed for the abatement of organic pollutants [3, 4]. But, magnetite with formula MFe_2O_4, where M represents the metallic cations like Fe, Co, Ni, Cu, Mg and Mn, has attracted a great deal of attention in the remediation of organic pollutants [5, 6]. The inverse spinel structure of $CoFe_2O_4$ suggests that Co^{2+} ions occupy octahedral site and Fe^{2+}& Fe^{3+} ions are equally distributed between tetrahedral and octahedral sites [7 - 9]. The current work focuses on the enhancement of visible light absorption and subsequent photocatalytic activities using ferrite compounds. Considering the adverse effect and complex structure of MB, we have carried out photocatalytic activity of Ce and Dy substituted $CoFe_2O_4$ using MB as a model pollutant under visible light irradiation.

2. MATERIALS AND METHODS

Photocatalytic Experiment.

Methylene blue was used as a model pollutant to evaluate the efficiency of the prepared Ce and Dy doped cobalt ferrites through the citrate-gel auto-combustion method [10]. The photocatalytic activity of the prepared samples was investigated by studying the decomposition of MB under visible light irradiation. A 500 W tungsten lamp was used as a visible light source, which is vertically placed inside an immersion well photochemical reactor made of Pyrex glass. Typically, 180 mg of photocatalyst was ultrasonically dispersed in 180 mL of an aqueous solution of MB and was stirred under dark for 30 min to maintain the adsorption-desorption equilibrium between the catalyst and MB. The temperature of the photochemical reactor was maintained by circulating the cold water through the inner jacket of reaction vessel in order to avoid any thermal reaction. After the adsorption-desorption process, the lamp was switched on and 5 mL aliquots were taken out at 15 min of time intervals and then, centrifuged at 6000 rpm to remove the catalyst from the solution. The concentration of MB was monitored by following the reduction in absorption intensity of MB at $\lambda_{max=}$ 663 nm using Perkin Elemer UV-Vis spectrophotometer (Lambda 35). The degradation efficiency of samples was determined using theexpression: Degradation efficiency = $(C_o-C_t)/C_o*100\%$, where C_o is the initial concentration of MB after adsorption-desorption equilibrium and C_t is the concentration of MB at different time intervals, respectively. The structure of $CoFe_2O_4$ was analyzed by X-ray diffractometer (XRD Rigaku, Cu-K_α λ=1.5418 Å). Further the Transmission Electron Microscope (TEM: Model Tecnai G20, FEI, USA), and Vibrating Sample Magnetometer (EV-7 VSM with Max. applied field $\pm$15 kOe) were used for morphological, and low temperature magnetic properties respectively.

3. RESULTS

Fig.1a represents XRD pattern of single phase cubic spinel $CoFe_2O_4$ and is consistent with standard JCPDS:22-1086. There were no secondary phases in diffraction pattern and hence confirmed high phase purity of $CoFe_2O_4$. The average crystallite size was calculated to be 56 nm indicating the presence of broad peak in XRD pattern (inset Fig.1.). The detailed structural parameters of Ce and Dy doped $CoFe_2O_4$ have already described in our previous work [10].

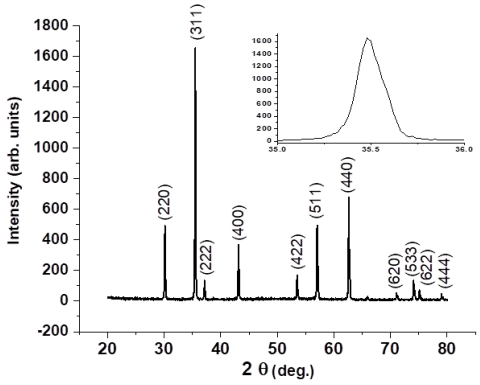

Figure 1. (a) XRD pattern of pure cobalt ferrite.

Fig.1b & c shows TEM micrographs of the prepared $CoCe_xDy_xFe_{2-2x}O_4$ (x=0.02 and 0.04) with selected area electron diffraction (SEAD) depicted in Fig.1d. The particle size was noted to be altering from ~ 20 to 50 nm. It was evident that well defined spherical and agglomerated nanoparticles were seen as a result of magnetic interactions among the nanoparticles [11]. The SAED pattern indicates polycrystalline nature of nanoferrites and formation of bright rings refers to different diffraction planes in unit cell.

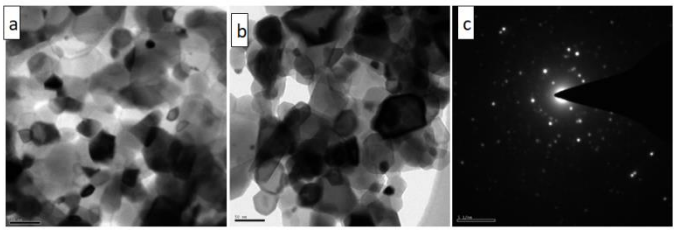

Figure 1. TEM pictures of $CoCe_xDy_xFe_{2-2x}O_4$ (b) x = 0.02, (c) x=0.04 and (d) SEAD of x = 0.02.

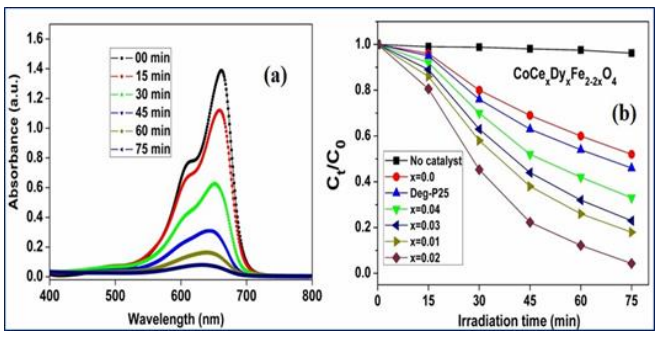

Figure 2. UV-Vis absorption spectra of MB in presence of $CoCe_xDy_xFe_{2-2x}O_4$ (x=0.02) (a) and (b) change in concentration of MB in presence of different samples under visible light irradiation.

The absorption spectra of MB centred at 663 nm versus irradiation time in the presence of $CoCe_xDy_xFe_{2-2x}O_4$ (x=0.02) is shown in Fig.2a. It is seen from figure that the absorption intensity of MB reduces with increase in irradiation time, manifesting the degradation of MB with irradiation time. During the experiments, we observed that the colour of MB changed to light blue and eventually to a clear solution with degradation process. The decolourization of MB is not an indication of mineralization as it may be converted to a colourless substances [12, 13]. The change in concentration of MB as a function of time in the presence of as-prepared samples is shown in Fig. 2b. The results indicate that MB cannot be degraded without the assistance of photocatalysis process and its self-decomposition is only 4% within 75 min of illumination time in the absence of catalyst [14–16]. Compared to undoped cobalt ferrite, Ce and Dy modified $CoFe_2O_4$ exhibited enhanced photocatalytic activity, indicating that recombination is quenched after adding Ce and Dy into cobalt ferrite. It is noted from figure that photocatalytic activity increases with increasing Ce and Dy up to x=0.02 and any further increment after the optimal level leads to a decrease in photocatalytic activity. The best activity was observed when the doping content of Ce and Dy was 0.02, for which 94.3 % of MB was decolorized in 75 min of irradiation. The enhanced photocatalytic activity is described based on a fact that space charge region becomes narrower which results in efficient separation of charge carriers within the region. At high loading content, the electron hole pair recombines quickly and making the photocatalytic activity of catalysts is ineffective. The results infer that optimal loading could provide a better separation of charge carriers and substantial light harvesting ability to the catalyst. These factors are responsible for photocatalytic activity of co-modified $CoFe_2O_4$ towards degradation of MB. The photocatalytic performance of samples was compared with Degussa P25, which is benchmark photocatalytic material having two phases such as anatase and rutile, under the analogous conditions and its result is shown in the same figure. The results demonstrate that Degussa P25 showed better activity than that of pure cobalt ferrite and could degrade MB 48% within 75 min of irradiation. In spite of having large bandgap energy, Degussa P25 showed better activity than pure $CoFe_2O_4$. The phase junction in TiO_2 is responsible for the better activity of Degussa P25 [17]. The presence of anatase & rutile phase increases electron transfer rate and further increases life time of photogenerated charge carriers thereby enhancing photocatalytic activity.

The kinetics of photodegradation process was further explored to better compare photocatalytic performance of samples. The apparent pseudo first order kinetics model based on Langmuir−Hinshelwood was applied [18], which is shown in equation: $\ln(C_0/C_t) = K_{app}t$, where k_{app}-apparent pseudo-first-order rate constant (min^{-1}), C_0-initial MB concentration (mg/L), and C_t-concentration of MB solution at time t (mol/L). The apparent rate constants of different samples are shown in Fig.2c. It is clear from

the figure that $CoCe_xDy_xFe_{2-2x}O_4$ with x=0.02 exhibits maximum rate constant for degradation of MB than that of other samples. The enhanced photocatalytic activity is credited to effective separation of charge carriers and enhanced visible light absorption ability.

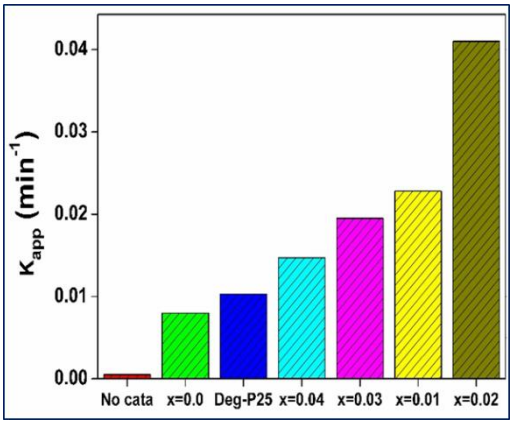

Figure 2. (c) Rate constants for the degradation of MB over different samples.

The magnetization behavior of $CoCe_xDy_xFe_{2-2x}O_4$ is studied using FC and ZFC under magnetic field (100 Oe) as shown in Fig.3. At first, sample was cooled to 75 K without applied magnetic fields. Secondly, measurements start from this temperature and sample was heated with an applied external magnetic field (100 Oe) and magnetization was measured with temperature. The magnetization of FC and ZFC curves coincide with each other in temperature near 300 K for x=0.02 and 0.04 compositions. It is seen that blocking temperature increases with increasing x. The ZFC curves increase with heating sample and reach to maximum at T_B called blocking temperature is higher than room temperature for all samples.

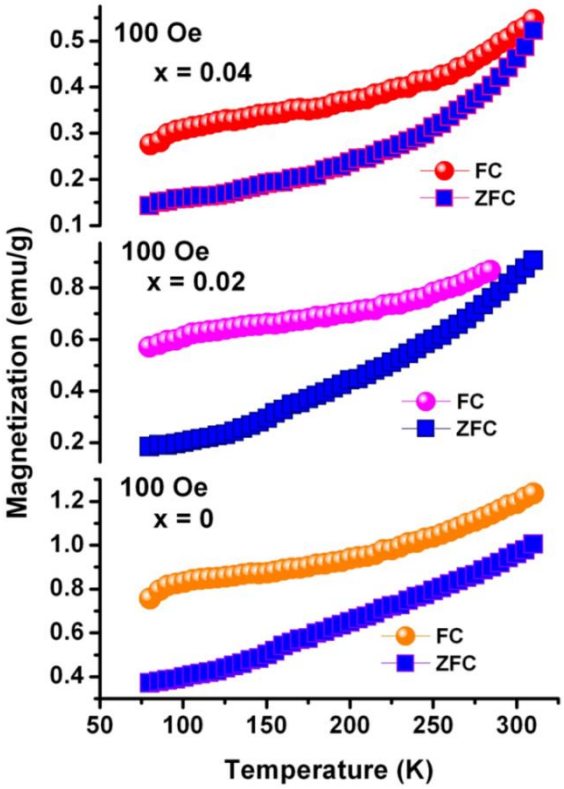

Figure 3. Magnetization of FC and ZFC for $CoCe_xDy_xFe_{2-2x}O_4$ (x = 0, 0.02, and 0.04) samples.

If magnetization of FC below T_B increases continuously, superparamagnetic state is formed, while the super-spin glass transition shows a very slow increase or a flat nature of the magnetization of FC mode at low temperatures [19]. Thus, the flat nature of the magnetization of FC curve below T_B (Fig.3) demonstrates super-spin glass behaviour of $CoCe_xDy_xFe_{2-2x}O_4$.

4. CONCLUSIONS

Single phase Ce and Dy doped cobalt nanoferrites were synthesized via citrate-gel auto-combustion method. TEM images confirmed the particle size below 50 nm. The photocatalytic efficiency of x = 0.02 composition towards the degradation of MB was found to be higher than pure cobalt nanoferrites. Magnetization was decreased with increasing Ce-Dy doping. The prepared $CoCe_xDy_xFe_{2-2x}O_4$ behaves like super-spin glass.

5. REFERENCES

1. Khanchandani, S.; Kumar, S.; Ganguli, A.K. Comparative Study of TiO_2/CuS Core/Shell and Composite Nanostructures for Efficient Visible Light Photocatalysis. *ACS Sustain. Chem. Eng.* **2016**, *4*, 1487–1499. https://doi.org/10.1021/acssuschemeng.5b01460.

2. Herrmann, J.M.; Duchamp, C.; Karkmaz, M.; Hoai, B.T.; Lachheb, H.; Puzenat, E.; Guillard, C. Environmental green chemistry as defined by photocatalysis. *Journal of Hazardous Materials.* **2007**, *146*, 624-629. https://doi.org/10.1016/j.jhazmat.2007.04.095.

3. Saison, T.; Chemin, N.; Chanéac, C.; Durupthy, O.; Ruaux, V.; Mariey, L.; Mauge, F.; Beaunier, P.; Jolivet, J.P. Bi_2O_3, $BiVO_4$, and Bi_2WO_6: Impact of Surface Properties on Photocatalytic Activity under Visible Light. *J. Phys. Chem. C* **2011**, *115*, 5657–5666. https://doi.org/10.1021/jp109134z.

4. Luan, J.; Shen, Y.; Zhang, L.; Guo, N. Property Characterization and Photocatalytic Activity Evaluation of $BiGdO_3$ Nanoparticles under Visible Light Irradiation. *Int. J. Mol. Sci.* **2016**, *17*, 1441, https://doi.org/10.3390/ijms17091441.

5. Naresh, U.; Kumar, R.J.; Naidu, K.C.B. Hydrothermal synthesis of barium copper ferrite nanoparticles: Nanofiber formation, optical, and magnetic properties. *Mater. Chem. Phys.* **2019**, *236*, 121807, https://doi.org/10.1016/j.matchemphys.2019.121807.

6. Ismail, M.M.; Jaber, N.A. Influences of cation distribution of zinc substituted on inverse spinel nickel ferrite nanoparticle for superparamagnetic approach. *Surf. Rev. let.* **2018**, *25*, 1850076, https://doi.org/10.1142/S0218625X18500762.

7. Rafeeq, S.N.; Ismail, M.M.; Sulaiman, J.M.A. Magnetic and Dielectric Properties of $CoFe_2O_4$ and $Co_xZn_{1-x}Fe_2O_4$ Nanoparticles Synthesized Using Sol-Gel Method. *J Magn*, **2017**, *22*, 406–413. https://doi.org/10.4283/JMAG.2017.22.3.406.

8. Vinuthna, C H, Naidu, K.C.B.; Chandra, S.C.; Ravinder D. Magnetic and Antimicrobial Properties of Cobalt Zinc Ferrite Nanoparticles Synthesized By Citrate-Gel Method. *Inter. J. Appli. Ceram. Techn.*, **2019**, *16*, 1944–1953, https://doi.org/10.1111/ijac.13276.

9. Boda, N.; Boda, G.; Naidu, K.C.B.; Srinivas, M.; Batoo, K.M.; Ravinder, D. Reddy, A.P. Effect of Rare Earth Elements

on Low Temperature Magnetic Properties of Ni and Co-Ferrite Nanoparticles. *J. Magn. Magn. Mater.* **2019**, *473*, 228-235, https://doi.org/10.1016/j.jmmm.2018.10.023.

10. Hashim, M.; Raghasudha, M.; Meena, S.S.;Shah, J.;Shirsath, S.E.; Kumar, S.; Ravinder, D.; Bhatt, P.; Kumar, R.; Kotnala, R.K. Influence of rare earth ion doping (Ce and Dy) on electrical and magnetic properties of cobalt ferrites. *J. Magn. Magn. Mater.* **2018**, *449*, 319-327. https://doi.org/10.1016/j.jmmm.2017.10.023.

11. Kumar, N.S.; Suvarna, R.P; Naidu, K.C.B. Grain and grain boundary conduction mechanism in sol-gel synthesized and microwave heated $Pb_{0.8-y}La_yCo_{0.2}TiO_3$ (y = 0.2-0.8) nanofibers. *Mater. Chem. Phys.* **2019**, *223*, 241-248, https://doi.org/10.1016/j.matchemphys.2018.11.004.

12. Manohar, A.; Krishnamoorthy, C.; Chandra Babu Naidu, K. Dielectric, Magnetic hyperthermia and Photocatalytic Properties of $ZnFe_2O_4$ Nanoparticles Synthesized by Solvothermal Reflux method, Applied Physics A, **2019,** *125*, 477, https://doi.org/10.1007/s00339-019-2760-0.

13. Srilakshmi, C.; Saraf, R.; Shivakumara, C.; Structural Studies of Multifunctional $SrTiO_3$ Nanocatalyst Synthesized by Microwave and Oxalate Methods: Its Catalytic Application for Condensation, Hydrogenation, and Amination Reactions. *ACS Omega* **2018**, *3*, 10503−10512, https://doi.org/10.1021/acsomega.8b01255.

14. Alam, U.; Khan, A.; Raza, W.; Khan, A.; Bahnemann, D.; Muneer, M. Highly efficient Y and V co-doped ZnO photocatalyst with enhanced dye sensitized visible light photocatalytic activity. *Catal. Today.* **2017**, *284*, 169–178. https://doi.org/10.1016/j.cattod.2016.11.037.

15. Alam, U.; Fleisch, M.; Kretschmer, I.; Bahnemann, D.; Muneer, M. One-step hydrothermal synthesis of Bi-TiO_2 nanotube/graphene composites: An efficient photocatalyst for spectacular degradation of organic pollutants under visible light irradiation. *Appl. Catal. B Environ.* **2017**, *218*, 758–769. https://doi.org/10.1016/j.apcatb.2017.06.016.

16. Alam, U.; Kumar, S.; Bahnemann, D.; Koch, J.; Tegenkamp, C. et al., Harvesting visible light with MoO_3nanorods modified by Fe(III) nanoclusters for effective photocatalytic degradation of organic pollutants. *Phys. Chem. Chem. Phys.***2018**, *20*, 4538–4545, https://doi.org/10.1039/C7CP08206A.

17. Kafizas, A.; Wang, X.; Pendlebury, S.R.; Barnes, P.; Ling, M.; et al., Spectroscopic and Polarization-Dependent Single-Molecule Tracking Reveal the One-Dimensional Diffusion Pathways in Surfactant-Templated Mesoporous Silica. *J. Phys. Chem.A.* **2016**, *120*, 715–723.

18. Huang, H.; Liu, K.; Chen, K.; Zhang, Y.; Zhang, Y.; Wang, S. Ce and F Comodification on the Crystal Structure and Enhanced Photocatalytic Activity of Bi_2WO_6 Photocatalyst under Visible Light Irradiation. *J. Phys. Chem. C* **2014**, *118*, 14379–14387.

19. Ramaprasad, T.; Kumar, R.J.; Naresh, U.; Prakash, M.; Kothandan, D.; Chandra, B.N.K. Effect of pH Value on Structural and Magnetic Properties of $CuFe_2O_4$ Nanoparticles Synthesized by Low Temperature Hydrothermal Technique. *Materials Research Express* **2018**, *5*, 095025, https://doi.org/10.1088/2053-1591/aad860.

6. ACKNOWLEDGEMENTS

The authors express thankful to Prof. D. Ravinder for taking care of work.